Many-body model of rare gases at high pressures

Eugene Pechenik and Itzhak Kelson
School of Physics and Astronomy, The Raymond and Beverly Sackler Faculty of Exact Sciences, Tel Aviv University, Tel Aviv 69978, Israel

Guy Makov
Department of Physics, NRCN, P.O. Box 9001, Beer Sheva 84190, Israel

(Received 27 September 2007; revised manuscript received 7 August 2008; published 27 October 2008)

An embedded atom type many-body model for describing rare-gas solids is developed. Model parameters are obtained by fitting zero-temperature compression curves, bulk moduli, and C_{44} elastic constants to experimental and *ab initio* data. The model is then used to calculate the pressure-dependent elastic constants, Cauchy discrepancies, and melting curves of Ne, Ar, Kr, and Xe. It is shown that a spherically symmetric many-body model cannot reproduce the high-pressure elastic properties of the system. The model successfully reproduces the experimentally observed negative Cauchy discrepancies and improves the agreement of the melting curves of rare-gas solids compared to pair-interacting calculations. The reported cusps on the melting curves of rare-gas solids have not been reproduced.

DOI: 10.1103/PhysRevB.78.134109 PACS number(s): 61.50.Lt, 62.20.D−, 62.50.−p, 64.70.D−

I. INTRODUCTION

Rare gases have been among the most widely studied materials, both experimentally and theoretically.[1] The importance of rare gases lies in the fact that they are a relatively simple system to study due to their closed-shell electronic structure. Of special interest are the high-pressure properties of rare gases because of their importance for geophysical research[2] and extensive use as a pressure medium in high-pressure diamond anvil cell experiments.[3] Some examples of experimentally measured high-pressure properties of rare gases are the compression curves of Xe,[4–6] Kr,[2,7,8] Ar,[9–11] and Ne,[9,12] the elastic properties of Kr,[7,13] Ar,[11] and Ne[14], pressure-induced phase transitions in Xe (Refs. 15–18) and Kr,[18] phonon-dispersion curves of Ar,[19] and the melting curves of Ne,[20] Ar,[21,22] Kr,[2,22] and Xe.[22,23] There have also been extensive studies of He properties, but because they are dominated by quantum effects, these are beyond the scope of the present paper.

At ambient conditions, rare gases are dominated by pair interactions. As a result, much of the modeling of rare gases in condensed phases has been undertaken with empirical interatomic pair potentials. These include the simple (12-6) Lennard-Jones[24] and (exp-6) Buckingham[25] pair potentials, modeling only the long-range van der Waals attraction and the short-range core-core repulsion, as well as the more complex potentials by Aziz and Chen,[26] Bobetic and Barker,[27] and others.

Despite the fact that rare gases in ambient conditions are characterized by pair interactions, experiments have shown that the high-pressure behavior of rare-gas solids deviates significantly from that of a simple pair-interacting solid. Grimsditch *et al.*[10] have shown that high-pressure argon possesses a negative Cauchy discrepancy $\delta=(C_{12}-C_{44})$, which increases in magnitude with pressure. Since the Cauchy discrepancy of a pair-interacting solid must be zero,[28] this finding suggests that rare gases possess many-body as well as two-body (pair) interactions and that the former become more significant at high-pressure conditions. This result has been recently confirmed by Shimizu *et al.*,[11] who studied high-pressure argon up to 70 GPa, and by several DFT calculations of high-pressure elastic properties of solid Ar (Ref. 29) and other rare-gas solids.[30]

The need for a many-body description of dense rare gases has been discussed in a number of works over the years (see Ref. 10, for example), and the main approach to this problem has been to correct the cohesive energy function, usually described by a sum over pair potentials, with physically motivated empirical three-body terms. This approach is taken by Loubeyre,[31,32] who combined the Aziz and Chen[26] pair potential with three-body terms originating from the Slater-Kirkwood exchange interaction and the Axilrod-Teller dispersion relation, and calculated the high-pressure equations of state of rare-gas solids. A more recent example of this approach is the work of Freiman and Tretyak,[33] who extended the equations of state of rare-gas solids to the megabar range. A notable success of Loubeyre's model is the prediction of an fcc-hcp transition at high-pressure in rare-gas solids.[32]

Despite these successes in modeling the cohesive energy, the high-pressure elastic properties of rare-gas solids remain beyond the scope of the abovementioned works. Recently Aoki and Kurokawa[34] proposed a many-body model that reproduces the high-pressure elastic properties of Ar, including the negative Cauchy discrepancy. The model is based on the nonorthogonal tight-binding theory and has no separate pair-interacting term describing repulsion.

An alternative many-body approach is the embedded atom method (EAM),[35] which is a semiempirical model mainly used to describe metals and alloys, as well as semiconductors, and covalently bonded elements. An important modification of this model is the modified embedded atom method (MEAM),[36] where many-body interactions are expanded in a series of three-body terms. In this formulation of EAM/MEAM, the many-body term affects the elastic and the thermal properties of the system, but not the cohesive energy, which is determined solely by the pair potential. This feature allows one to use a pair potential that best fits the equation of

state and to treat the many-body term as an empirical correction of the elastic properties. Another feature of EAM/MEAM models is their atomistic rather than geometric formulation, making them easier to employ in molecular-dynamics simulations.

Another interesting pressure-dependent property, not yet studied with many-body models and expected to depend on many-body effects, is the melting curve. Recent experiments by Boehler and co-workers[22,23] have shown cusps on the melting curves of Xe, Kr, and Ar at 16, 30, and 40 GPa, respectively. These cusps have not been found on the calculated melting curves of rare-gas solids using a variety of classical pair potentials and *ab initio* methods.[20,25,37–41]

In this work we develop an EAM based many-body potential for rare gases and apply it to study the high-pressure properties of rare-gas solids. The work is organized as follows. In Sec. II we first attempt to construct a spherically symmetric many-body EAM potential, which we show to be insufficient to describe the elastic properties of the system. Then we proceed to develop a model with three-body terms and explicit angular dependence. In Sec. III the model is fitted to the high-pressure compression curves and C_{44} elastic constants of rare-gas solids. Additional elastic properties, including the high-pressure Cauchy discrepancies, are then calculated. In Sec. IV we calculate the melting curves of rare-gas solids using molecular dynamics simulations and compare them to experimental data and other theoretical calculations. We conclude with a discussion of our results.

II. MODEL

A. Spherically symmetric many-body model

We begin by constructing a simple many-body model based on the EAM formalism.[35] In this formalism the energy of an atom is written as a sum of two terms: the embedding energy $F(\bar{\rho}_i)$, which is the many-body term, and the pair potential $\phi(r_{ij})$,

$$E_i = F_i(\bar{\rho}_i) + \frac{1}{2}\sum_{j\neq i}\phi(r_{ij}). \tag{1}$$

In the case of rare gases, the embedding energy term can be considered as an extension to the pair potential, which is the main potential term.

The embedding energy of an atom is a functional of the "average electron density" $\bar{\rho}_i$ at the atom site, defined as

$$\bar{\rho}_i = \frac{1}{Z}\sum_{j\neq i}\rho_{ij}, \tag{2}$$

where

$$\rho_{ij} = \exp[-\beta(r_{ij}/r_{1e}-1)], \tag{3}$$

and β and r_{1e} (equilibrium nearest-neighbor distance) are parameters of the potential. Z is the coordination number of the lattice ($Z_{\mathrm{fcc}}=12$). The ground-state phase of most rare-gas solids is fcc, and it is assumed that no phase transitions occur during compression. The embedding function is chosen as[35]

$$F_i(\bar{\rho}_i) = \frac{Z}{2}E_c A\bar{\rho}_i \ln(\bar{\rho}_i), \tag{4}$$

where E_c is the cohesion energy and A is a model parameter.

The pair potential is defined as

$$\phi(r_{ij}) = \phi^{\mathrm{PP}}(r_{ij}) - \frac{2}{Z}F_i(\rho_{ij}), \tag{5}$$

where ϕ^{PP} is a model pair potential. In this work we use the Lennard-Jones (12-6) and the Buckingham (exp-6) pair potentials. While both potentials have been widely used to describe rare gases at ambient conditions, the latter have been successfully applied to high-pressure conditions as well.[25] The two potentials are defined as follows:

$$\phi^{\mathrm{LJ}}(r_{ij}) = E_c[(r_{ij}/r_{1e})^{-12} - 2(r_{ij}/r_{1e})^{-6}],$$

$$\phi^{\mathrm{B}}(r_{ij}) = E_c\left[\frac{6}{\alpha-6}\exp[-\alpha(r_{ij}/r_{1e}-1)] - \frac{\alpha}{\alpha-6}(r_{ij}/r_{1e})^{-6}\right]. \tag{6}$$

Buckingham potential has an additional parameter α, which is associated with the bulk modulus. The resulting model has a total of five parameters (α included), three of which belong to the pair potential and are determined by the physical properties of the material being described, and two are free and belong to the many-body term. Note that parameter A is responsible for the relative strength of the many-body term and can be zero. In this special case the many-body term cancels, and only the pair potential remains.

Now we shall see whether the EAM model is able to produce a correct calculation of the Cauchy discrepancy, a property that is experimentally negative, but always zero for a pair potential. It can be shown that the Cauchy discrepancy of a perfect homonuclear crystal in a nearest-neighbor EAM model is[36]

$$\delta = \frac{F''(\bar{\rho})}{9V}[\rho'(r_1)r_1]^2, \tag{7}$$

where r_1 is the nearest-neighbor distance and V is the atomic volume, which is proportional to r_1^3. It can be easily seen that Eq. (7), which can be easily generalized for any number of neighbor shells, is positive definite, since $F''(\bar{\rho})$, which is the second derivative of the embedding energy, must be positive for the system to be stable. Therefore, for EAM, the Cauchy discrepancy is always positive and proportional to the curvature of the embedding energy function $F(\bar{\rho})$. This conclusion is valid not only for EAM, but for *any* spherically symmetric many-body model with $\bar{\rho}_i$ defined according to Eq. (2), i.e., consisting of two-body terms only. This result does not depend on the specific functional forms of ρ_{ij} and $F(\bar{\rho})$. We conclude that spherically symmetric EAM-like many-body models cannot provide an appropriate description of elastic properties of rare-gas solids.

B. Many-body model with explicit angular dependence

Having concluded that spherically symmetric many-body models are insufficient to describe the properties of rare-gas

solids, we introduce an explicit angular dependence into our model. The angular dependence is introduced in a way inspired by the MEAM model of Baskes.[36] We begin by replacing the original two-body terms of $\bar{\rho}_i$ in Eq. (2) with three-body terms and expanding in a geometric series of cosines as follows:

$$(\bar{\rho}_i)^2 = \frac{1}{Z^2}\sum_{\substack{j\neq i\\ k\neq i}} \rho_{ij}\rho_{ik}[a_0 + a_1\cos(\theta_{jik}) + a_2\cos^2(\theta_{jik}) + \cdots], \tag{8}$$

where a_n are real coefficients. The series can be rearranged to take the form of Legendre polynomials

$$(\bar{\rho}_i)^2 = \frac{1}{Z^2}\sum_{\substack{j\neq i\\ k\neq i}} \rho_{ij}\rho_{ik}[b_0P_0(x_{jik}) + b_1P_1(x_{jik}) + b_2P_2(x_{jik}) + \cdots], \tag{9}$$

where

$$P_0(x_{jik}) = 1,$$

$$P_1(x_{jik}) = x_{jik},$$

$$P_2(x_{jik}) = 3{x_{jik}}^2 - 1, \tag{10}$$

$x_{jik}=\cos(\theta_{jik})$, θ_{jik} is the angle formed between atoms j, i, and k, and b_n are real coefficients (similar to a_n). Legendre polynomials can be expressed in terms of interatomic distances as

$$P_0(x_{jik}) = 1,$$

$$P_1(x_{jik}) = \sum_\alpha \frac{r_{ij}^\alpha r_{ik}^\alpha}{r_{ij}r_{ik}},$$

$$P_2(x_{jik}) = 3\sum_{\alpha,\beta} \frac{r_{ij}^\alpha r_{ij}^\beta r_{ik}^\alpha r_{ik}^\beta}{(r_{ij}r_{ik})^2} - 1, \tag{11}$$

where r_{ij}^α are the projections of the interatomic distances r_{ij} on the axes of an arbitrary Cartesian system. (α,β) and (i,j,k) are dimensional and atomic indices, respectively. Using Eq. (11) and following Ref. 36, we rewrite Eq. (9) as

$$(\bar{\rho}_i)^2 = [b_0(\bar{\rho}_0)^2 + b_1(\bar{\rho}_1)^2 + 3b_2(\bar{\rho}_2)^2 + \cdots], \tag{12}$$

where

$$(\bar{\rho}_0)^2 = \frac{1}{Z^2}\left(\sum_{j\neq i}\rho_{ij}\right)^2,$$

$$(\bar{\rho}_1)^2 = \frac{1}{Z^2}\sum_\alpha\left(\sum_{j\neq i}\rho_{ij}\frac{r_{ij}^\alpha}{r_{ij}}\right)^2,$$

$$(\bar{\rho}_2)^2 = \frac{1}{Z^2}\left[\sum_{\alpha,\beta}\left(\sum_{j\neq i}\rho_{ij}\frac{r_{ij}^\alpha r_{ij}^\beta}{{r_{ij}}^2}\right)^2 - \frac{1}{3}\left(\sum_{j\neq i}\rho_{ij}\right)^2\right]. \tag{13}$$

It should be pointed out that the terms of Eq. (13) are independent of the particular choice of a coordinate system.

Now, with the angular terms defined, we look for the lowest-order term that is capable of reproducing a negative Cauchy discrepancy. The zero-order term, which is the spherically symmetric term (2) discussed in Sec. II A, contributes positively to the Cauchy discrepancy and, therefore, cannot be used. The first-order term has no effect on the elastic properties, as it cancels for any structure with inversion symmetry. The lowest-order angular term that matches our criteria is, therefore, the second-order term. We choose it to represent the angular dependence in our model and for simplicity set b_0 and b_1 to zero. Without losing generality, b_2 is set to $1/3$, and the average electron density $\bar{\rho}_i$ is now written as

$$\bar{\rho}_i = \frac{1}{Z}\sqrt{\sum_{\alpha,\beta}\left(\sum_{j\neq i}\rho_{ij}\frac{r_{ij}^\alpha r_{ij}^\beta}{{r_{ij}}^2}\right)^2 - \frac{1}{3}\left(\sum_{j\neq i}\rho_{ij}\right)^2}. \tag{14}$$

For an undisturbed cubic lattice, $\bar{\rho}_i$ becomes zero, and the functional form of the embedding function, as formulated in Eq. (4), can no longer be used. Therefore, we modify the embedding function slightly so it will not diverge at low values of $\bar{\rho}_i$,

$$F_i(\bar{\rho}_i) = \frac{Z}{2}E_cA\bar{\rho}_i\ln(\bar{\rho}_i + 1). \tag{15}$$

The pair potential (5) is modified as well and becomes simply

$$\phi(r_{ij}) = \phi^{\mathrm{PP}}(r_{ij}), \tag{16}$$

where $\phi^{\mathrm{PP}}(r_{ij})$ is a model pair potential defined in Eq. (6).

The resulting many-body model has five parameters, which are identical to those of the spherically symmetric EAM model described in Sec. II A. In Sec. III we obtain the model parameters by calculating the zero-temperature properties of rare-gas solids and fitting the results to available *ab initio* and experimental data.

III. ZERO-TEMPERATURE PROPERTIES AND PARAMETER FITTING

A. Zero-temperature compression curves

The zero-temperature compression curves are calculated by minimizing the energy of a crystal with respect to its volume at a given pressure. The interactions are calculated up to the second-nearest neighbors for the entire pressure range. This condition is satisfied by a varying-distance cutoff function, calculated according to the following formula:

$$r_c = r_c^0(V/V_0)^{1/3}. \tag{17}$$

Here $r_c^0=1.573$ is the zero-pressure cutoff distance, defined as the halfway distance between the second- and the third-nearest neighbors in an fcc crystal. Here the zero-pressure nearest-neighbor distance is defined as 1.0. V and V_0 are the

TABLE I. Model parameters of Buckingham and LJ potentials, obtained by fitting calculated zero-temperature compression curves to experimental compression curves of various rare-gas solids.

	α	r_{1e} (Å)	T_0 (K)
Xe	12.1	4.53	235.0
Kr	12.5	4.12	175.0
Ar	12.0	4.00	122.0
Ne	12.8	3.25	42.0
(LJ) Ar		3.75	119.5

current and the zero-pressure system volumes, respectively.

In case of an ideal cubic crystal under uniform compression the many-body term cancels, so the zero-temperature compression curves depend only on the pair potential. Therefore, the latter can be used to obtain the model parameters of the pair potential—E_c, r_{1e}, and α. Note that the cohesion energy is presented in units of temperature as $T_0=E_c/k_B$, where k_B is the Boltzmann constant.

The final parameters for Ne, Ar, Kr, and Xe are listed in Table I. The compression curves, calculated with parameters from Table I and compared to experimental data,[2,5–7,10–12,16,17] *ab initio* results,[29] three-body[33] and two-body[42] model calculations, appear in Figs. 1–4. It should be noted that the experimental curves were measured at room temperature. In order to evaluate the thermal pressure contribution to the compression curves, we performed a constant-temperature molecular-dynamics simulation of Ar at 300 K with the full many-body model. As one can see in Fig. 2(a) (filled circles), the thermal contribution was found to be negligible.

The agreement between our calculations and the experimental and *ab initio* data is very good, as can be seen in Figs. 1(a), 2(a), 3(a), and 4(a). Let us recall that in our model the compression curves are not affected by the many-body term; they are the result of the pair potential only. In Fig. 4(a), one can see a small discrepancy between the hcp data (triangles) and the fcc results (filled circles and continuous line). It should be noted that in our calculations, as well as in the other theoretical calculations referenced here, all rare gases are treated as fcc for the entire pressure range.

While there is an excellent agreement between results obtained with the Buckingham potential and the experimental data, the Lennard-Jones potential appears to be much less successful. The discrepancy between the two potentials can be more easily seen on a logarithmic scale [Fig. 2(b)]. In the case of the Lennard-Jones potential, the pressure derivative of the bulk modulus, which is a function of E_c and r_{1e}, is greatly overestimated. In the case of the Buckingham potential, the additional parameter α allows a more accurate fitting of the pressure derivative of the bulk modulus and, as a result, a better agreement with the experimental compression curves. Following these results we focus mainly on the Buckingham potential in the following calculations.

At very high pressures, beyond the experimental range, our results are compared to the three-body calculations by Freiman and Tretyak[33] and the pair-interacting model by Zarochentsev *et al.*[42] [Figs. 1(b)–4(b)]. All three models are comparable, with our results lying between the other two models. Freiman and Tretyak reported that their model fails above 250, 200, and 175 GPa for Ar, Kr, and Xe, respectively. In the calculated pressure range, we did not see any unphysical effects in our model. Below the above-mentioned pressures, our results agree with those of Freiman and Tretyak somewhat better than with those of Zarochentsev *et al.*

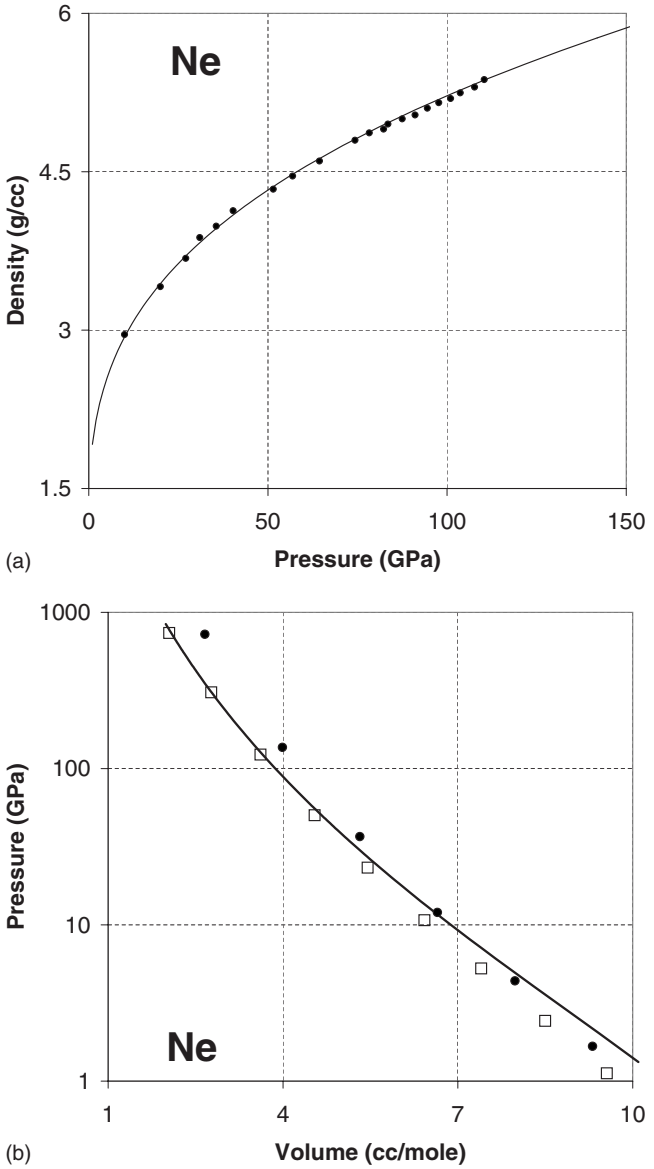

FIG. 1. (a) The compression curve of Ne, calculated with the current model at 0 K (solid line). Filled circles represent room-temperature experimental data from Ref. 12. (b) The compression curve of Ne [same as in (a)], compared to previous theoretical calculations. Open squares represent three-body model calculations from Ref. 33. Filled circles represent pair-interacting model results from Ref. 42.

B. Zero-temperature elastic properties

Pressure-dependent elastic constants are obtained by a numerical calculation of the second derivative of the system

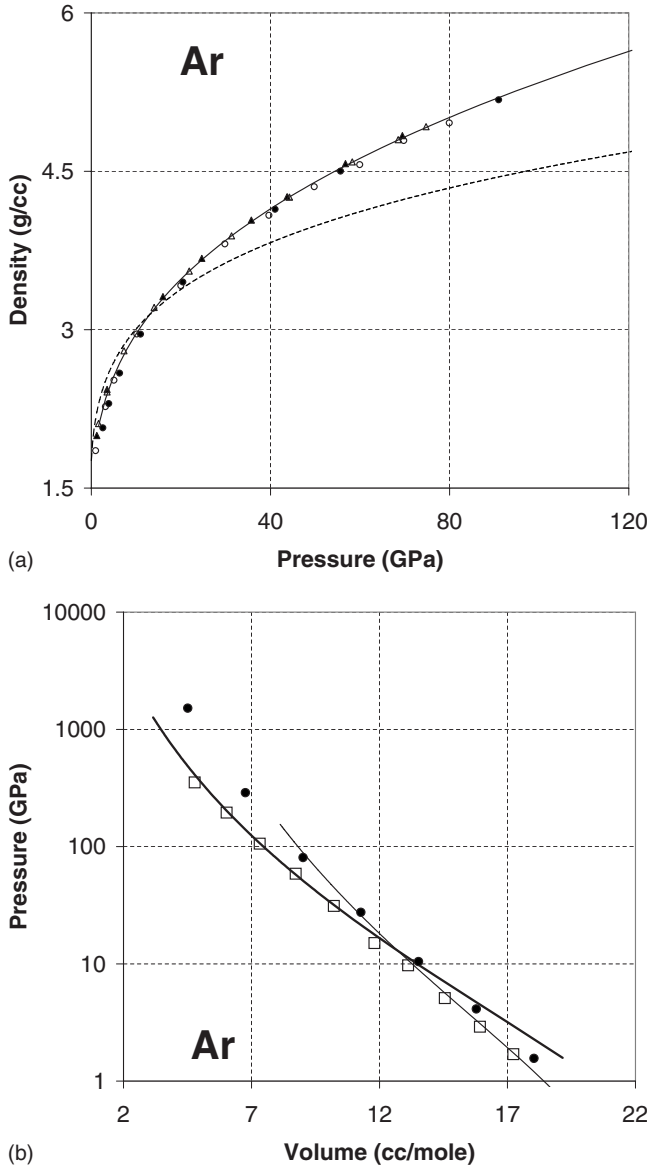

FIG. 2. (a) Compression curves of Ar, calculated with the current model (Buckingham potential) at 0 K (solid line) and 300 K (filled circles), and the LJ potential at 0 K (dashed line). Filled and empty triangles represent the room temperature experimental data from Refs. 10 and 11, respectively. Empty circles represent 0 K *ab initio* calculations from Ref. 29. The effect of the temperature can be seen to be negligible. LJ results deviate significantly from the experimental data. (b) Compression curves of Ar, calculated with the current model (Buckingham potential) at 0 K (solid line), and the LJ potential at 0 K (thin line), and compared to previous theoretical calculations. Open squares represent three-body model calculations from Ref. 33. Filled circles represent pair-interacting model results from Ref. 42.

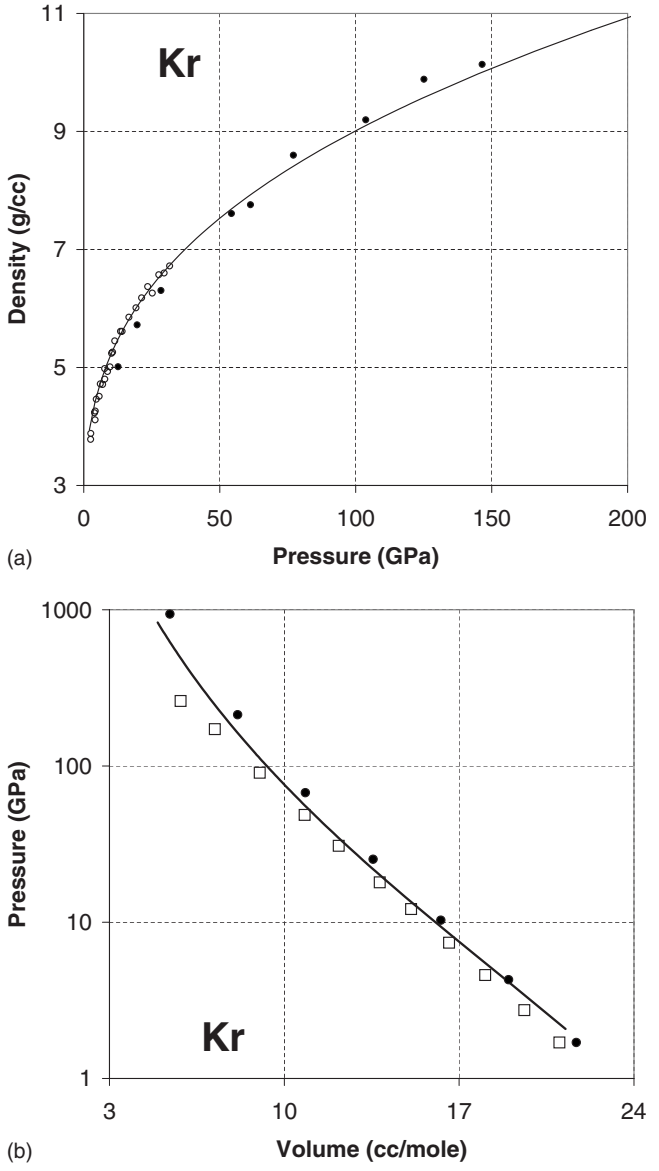

FIG. 3. (a) The compression curve of Kr, calculated with the current model at 0 K (solid line). Filled and open circles represent the room-temperature experimental data from Refs. 2 and 7, respectively. (b) The compression curve of Kr [same as in (a)], compared to previous theoretical calculations. Open squares represent three-body model calculations from Ref. 33. Filled circles represent pair-interacting model results from Ref. 42.

energy with regard to an appropriate infinitesimal strain. Exact formulae used to calculate the elastic constants can be found in the Appendix. Unlike the compression curves, which depend only on the pair potential, the elastic constants are affected by the many-body term and can be used to determine the remaining model parameters. As before, a second-nearest-neighbor varying-distance cutoff was used in these calculations.

For an isotropically compressed crystal, the experimentally measured stress-strain coefficients (the Birch moduli) B_{ij} are derived from the elastic constants C_{ij} as follows:

$$B_{11} = C_{11} - P,$$

$$B_{12} = C_{12} + P,$$

$$B_{44} = C_{44} - P, \tag{18}$$

with P being the applied isotropic pressure.[28] Additional quantities, such as the experimentally measured bulk modu-

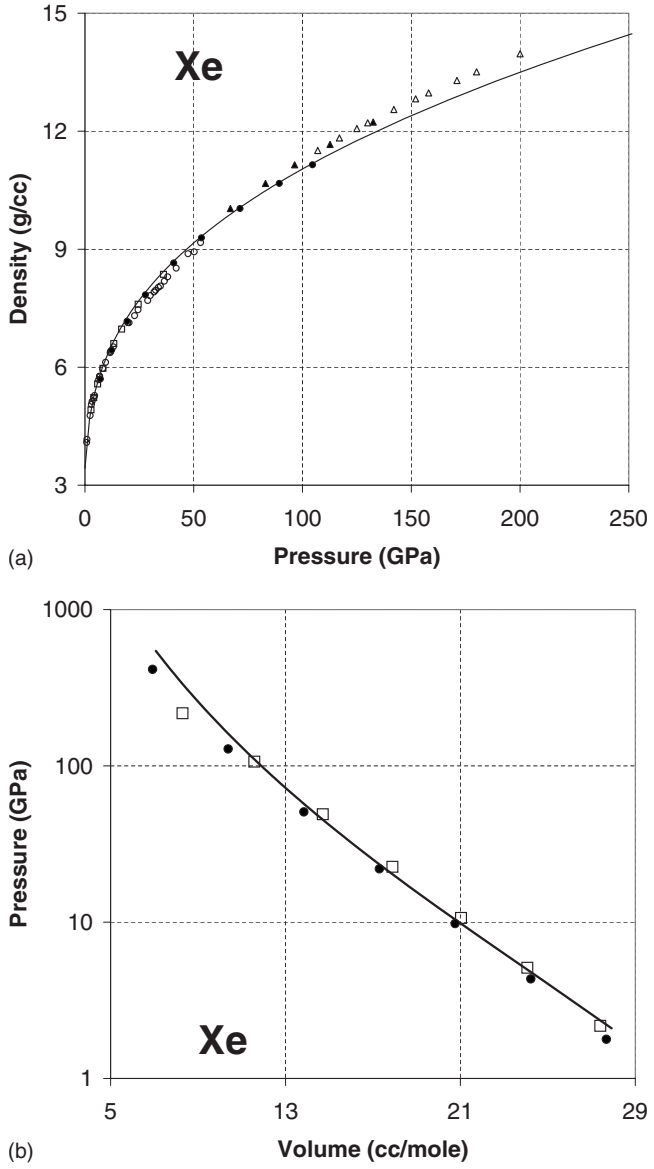

FIG. 4. (a) The compression curve of Xe, calculated with the current model at 0 K (solid line). Experimental results at room temperature are from Refs. 5 (open squares), 6 (open circles), 16 (open triangles), and 17 (filled circles and triangles). There is a small discrepancy between hcp experimental data, represented with triangles, and fcc results (the other data). (b) The compression curve of Xe [same as in (a)], compared to previous theoretical calculations. Open squares represent three-body model calculations from Ref. 33. Filled circles represent pair-interacting model results from Ref. 42.

lus B and the Cauchy discrepancy δ, can also be derived from the elastic constants

$$B = \frac{1}{3}(B_{11} + 2B_{12}) = \frac{1}{3}(C_{11} + 2C_{12} + P),$$

$$\delta = (B_{12} - B_{44}) - 2P = (C_{12} - C_{44}). \quad (19)$$

In the course of this work we found that except for B_{44}, which depends strongly on the many-body term, the differences between effective elastic constants calculated with and without the many-body term are negligible. We also found that B_{44}, being a monotonic function of A and β, is affected in a similar way by both many-body parameters. As a result, we chose to assign a nominal value of 1.0 to A, making it constant, and determine β by fitting the calculated B_{44} to *ab initio* and experimental data. The resulting values of β are listed in Table II.

TABLE II. The fitted model parameter β of the many-body term for various rare gases.

Ne	Ar	Kr	Xe
8.5	8.1	8.1	8.5

Effective bulk moduli, elastic constants, and Cauchy discrepancies of Ne, Ar, Kr, and Xe, calculated with the many-body model, Buckingham, and Lennard-Jones potentials (for Ar), and compared to *ab initio* calculations,[29,30] experimental data,[11,14] and recent many-body[34] and pair-interacting model calculations,[42] appear in Figs. 5–8. The many-body term affects mostly B_{44}, whereas considering the other elastic constants, there is virtually no difference between those calculated with the many-body model and the Buckingham potential alone.

The agreement between our model and the available experimental data for Ar and Kr depends on the calculated quantities. In the case of the bulk moduli B, the agreement is excellent. This agreement is the result of the good fit of the equations of state that determine the pressure dependence of the bulk moduli. This is especially important in the case of Ne and Xe, for which no high-pressure experimental data are available. The effective shear moduli B_{44} were corrected by the many-body term so they would agree with the experimental data in the case of Ar and Kr and with *ab initio* calculations for Ne and Xe. Considering the other elastic constants, B_{12} are slightly higher and B_{11} are slightly lower than experiment. The Cauchy discrepancies δ, calculated with our many-body model, are consistent with both *ab initio* and experimental data. Minor differences between the model δ and the reference data are probably caused by the small disagreement in B_{12}, which is an output of the model, and not by a fitted quantity, B_{44}.

Comparing our results to other theoretical calculations, one can see that our data have a negative curvature, making them progressively lower at very high pressures. Our results for Ar are consistent with the many-body model of Aoki and Kurokawa,[34] as can be seen in Fig. 6. In the case of the heavy rare gases, Kr and Xe, our many-body results are mostly consistent with both *ab initio* (Ref. 30) and pair-interacting model (Ref. 42) calculations. An exception is the B_{44} elastic constant of Xe from Ref. 42, which is more consistent with the Buckingham potential than with the many-body model result. In the case of Ne and Ar, the results of both Refs. 30 and 42 agree neither with our calculations, nor with the experimental data (for Ar), being constantly higher

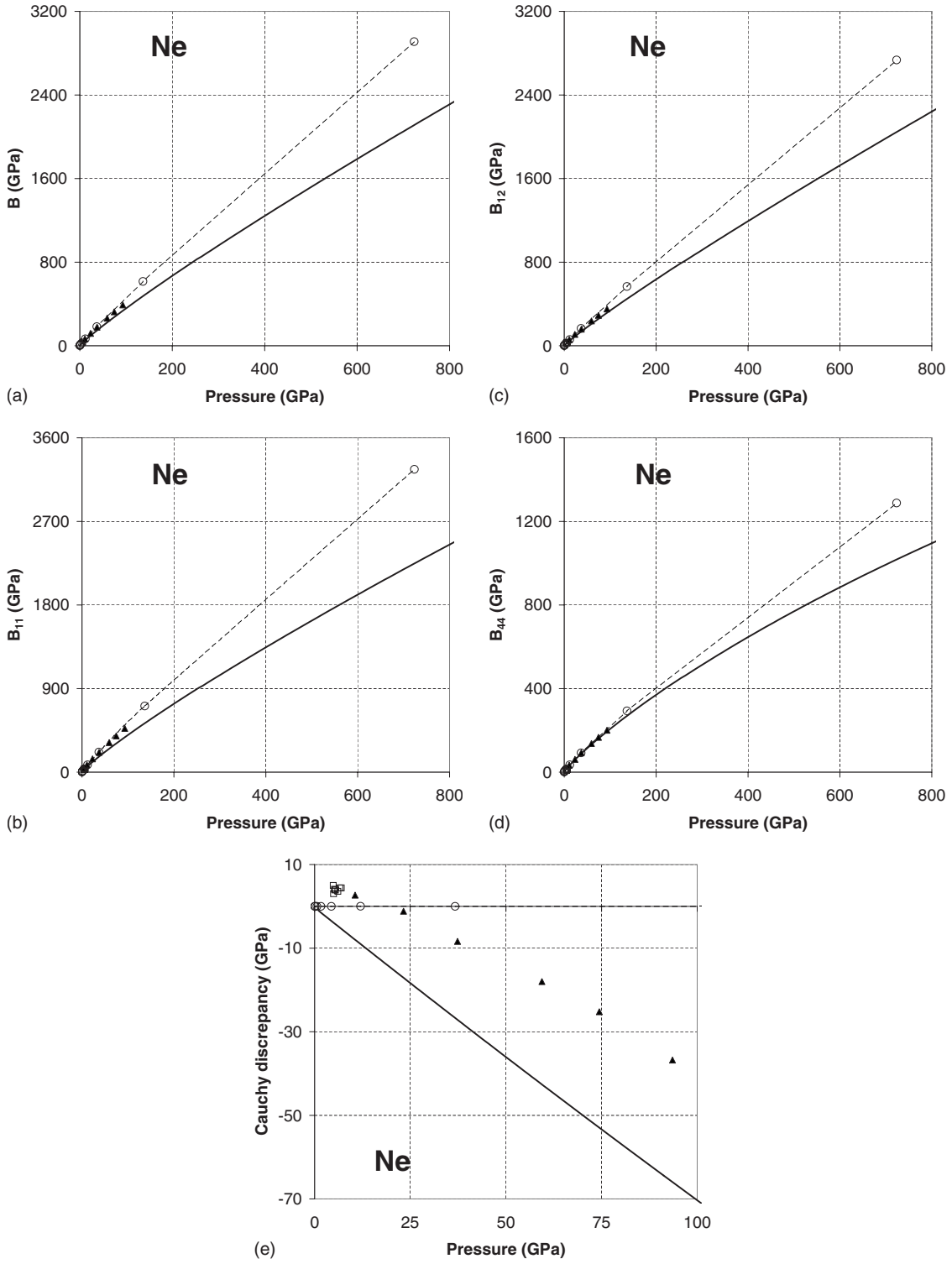

FIG. 5. Pressure-dependent effective elastic moduli [(a) B, (b) B_{11}, (c) B_{12}, (d) B_{44}] and the (e) Cauchy discrepancy of Ne, calculated with the many-body model at 0 K (solid line). The results are compared to 0 K *ab initio* calculations (Ref. 30—solid triangles), experimental data at room temperature (Ref. 14—open squares), and pair-interacting model calculations at 0 K (Ref. 42—dashed line).

than both. A possible reason for such behavior is the bulk modulus pressure derivative, which is overestimated in both calculations, as can be seen in Figs. 5(a) and 6(a). A similar behavior can be seen in our Lennard-Jones results, which also deviate from the experimental data (Fig. 6) because of an overestimated bulk modulus pressure derivative. It is interesting that our results and the results of Ref. 42 behave similarly, with B_{44} and B_{11} being lower, and B_{12} being higher than experimental and *ab initio* data. Obviously, the experimental Cauchy discrepancies, well described in *ab initio* and many-body model calculations, are not reproduced by any of the pair-potential models.

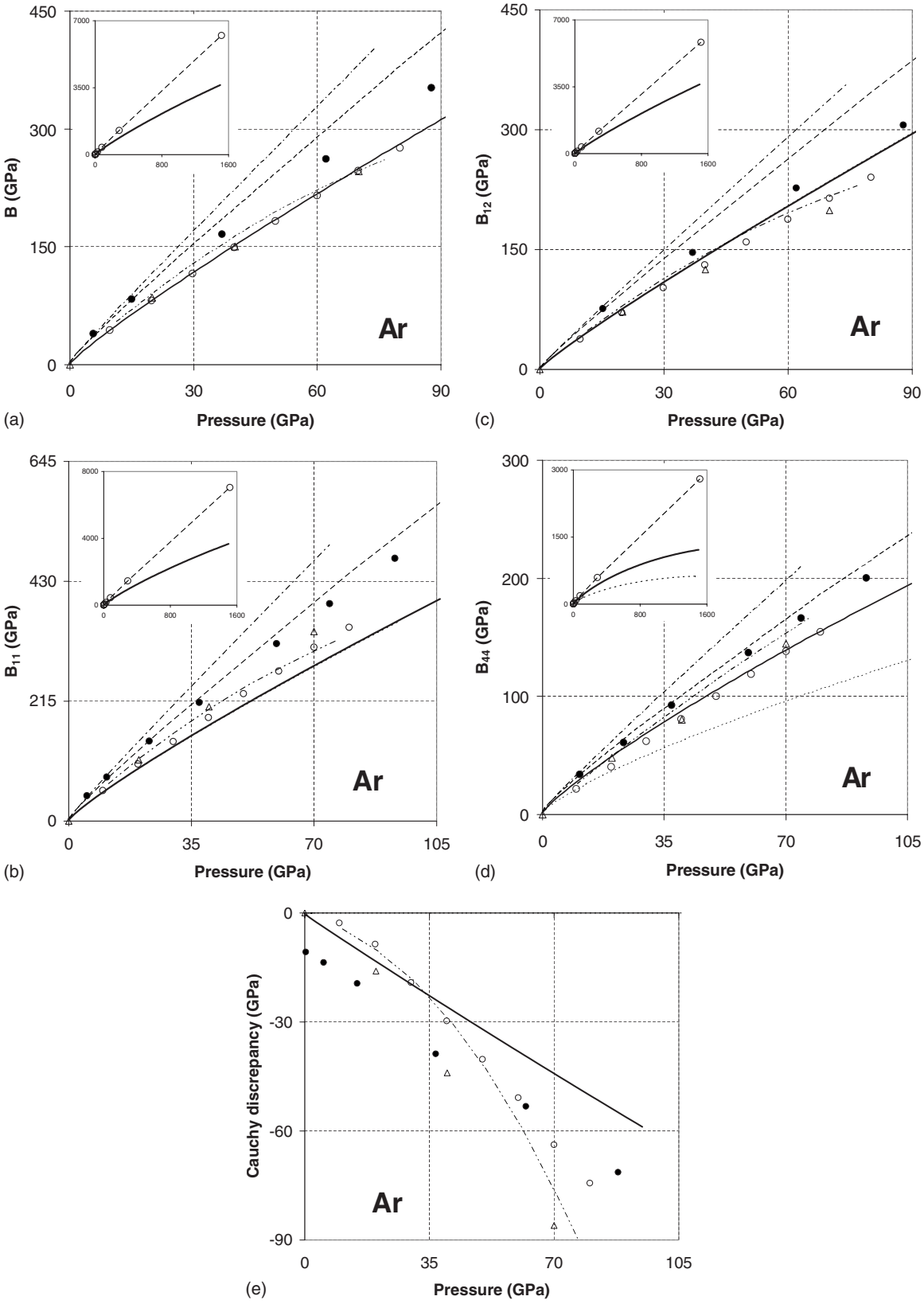

FIG. 6. Pressure-dependent effective elastic moduli [(a) B, (b) B_{11}, (c) B_{12}, (d) B_{44}] and the (e) Cauchy discrepancy of Ar, calculated with the many-body model (solid line), Buckingham (dotted line), and Lennard-Jones (dashed-dotted line) pair potentials at 0 K. The results are compared to 0 K *ab initio* calculations (Ref. 29—open circles; Ref. 30—solid circles), experimental data at 300 K (Ref. 11—open triangles), many-body model results at 0 K (Ref. 34—dashed-double dotted line), and pair-interacting model calculations at 0 K (Ref. 42—dashed line). The high-pressure results appear in the inset.

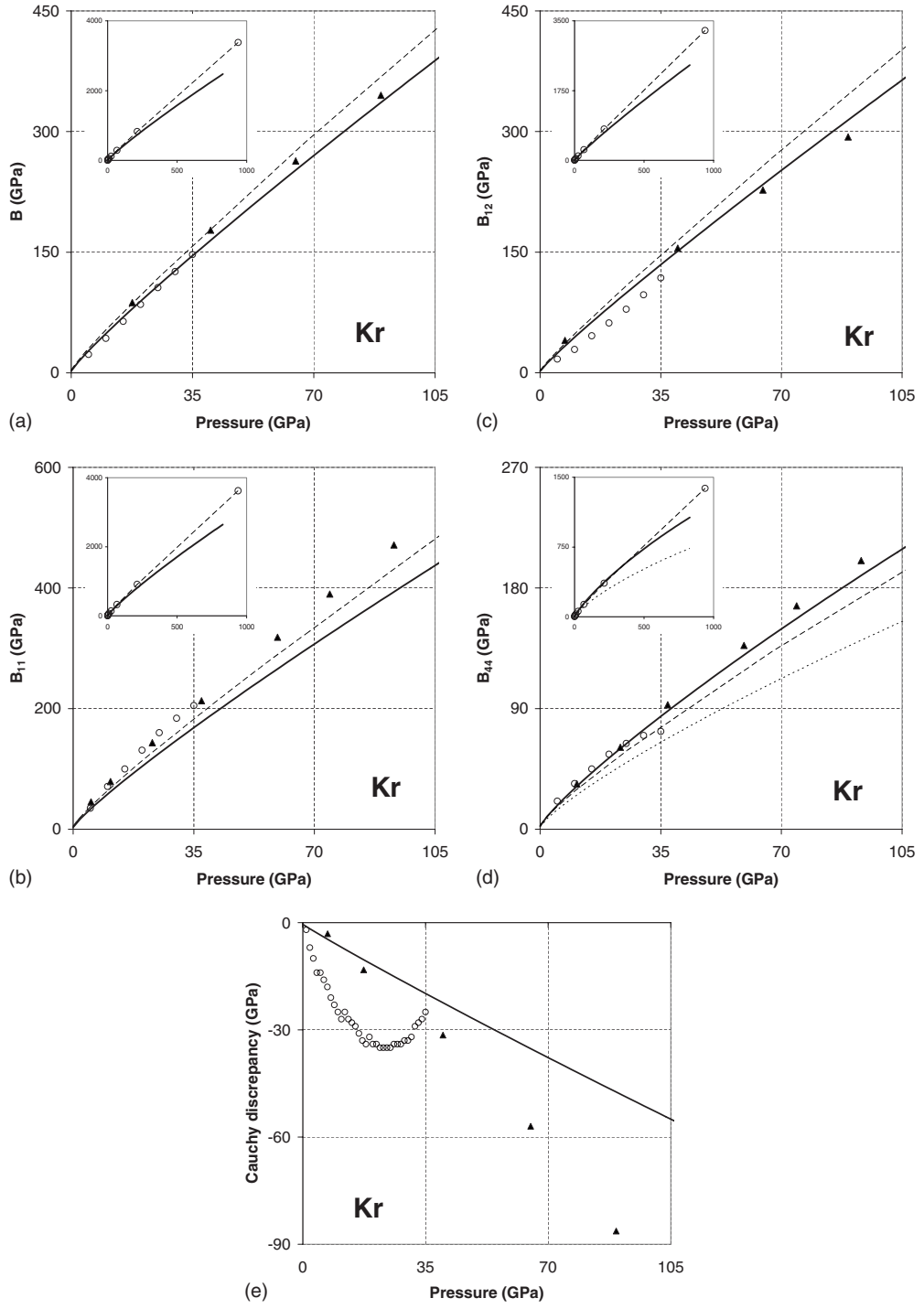

FIG. 7. Pressure-dependent effective elastic moduli [(a) B, (b) B_{11}, (c) B_{12}, (d) B_{44}] and the (e) Cauchy discrepancy of Kr, calculated with the many-body model (solid line) and the Buckingham pair potential (dotted line) at 0 K. The results are compared to 0 K *ab initio* calculations (Ref. 30—solid triangles), experimental data at room temperature (Ref. 7—open circles), and pair-interacting model calculations at 0 K (Ref. 42—dashed line). The high-pressure results appear in the inset.

IV. MELTING CURVE

In this section we apply our many-body model to calculate the melting curves of Ne, Ar, Kr, and Xe. The calculations are based on the moving interface method,[43] where a joint molecular-dynamics simulation of the solid and the liquid phases sharing an interface is performed. If the initial thermodynamic state of the system is within the mixed-phase region of the phase space, the system will be able to maintain equilibrium by changing slightly the volume of each phase, moving the interface between them. Otherwise, if the system is initially in the solid or the liquid region of the phase space, it will either completely melt or solidify during the simulation. The total number of atoms in the reported simulations is

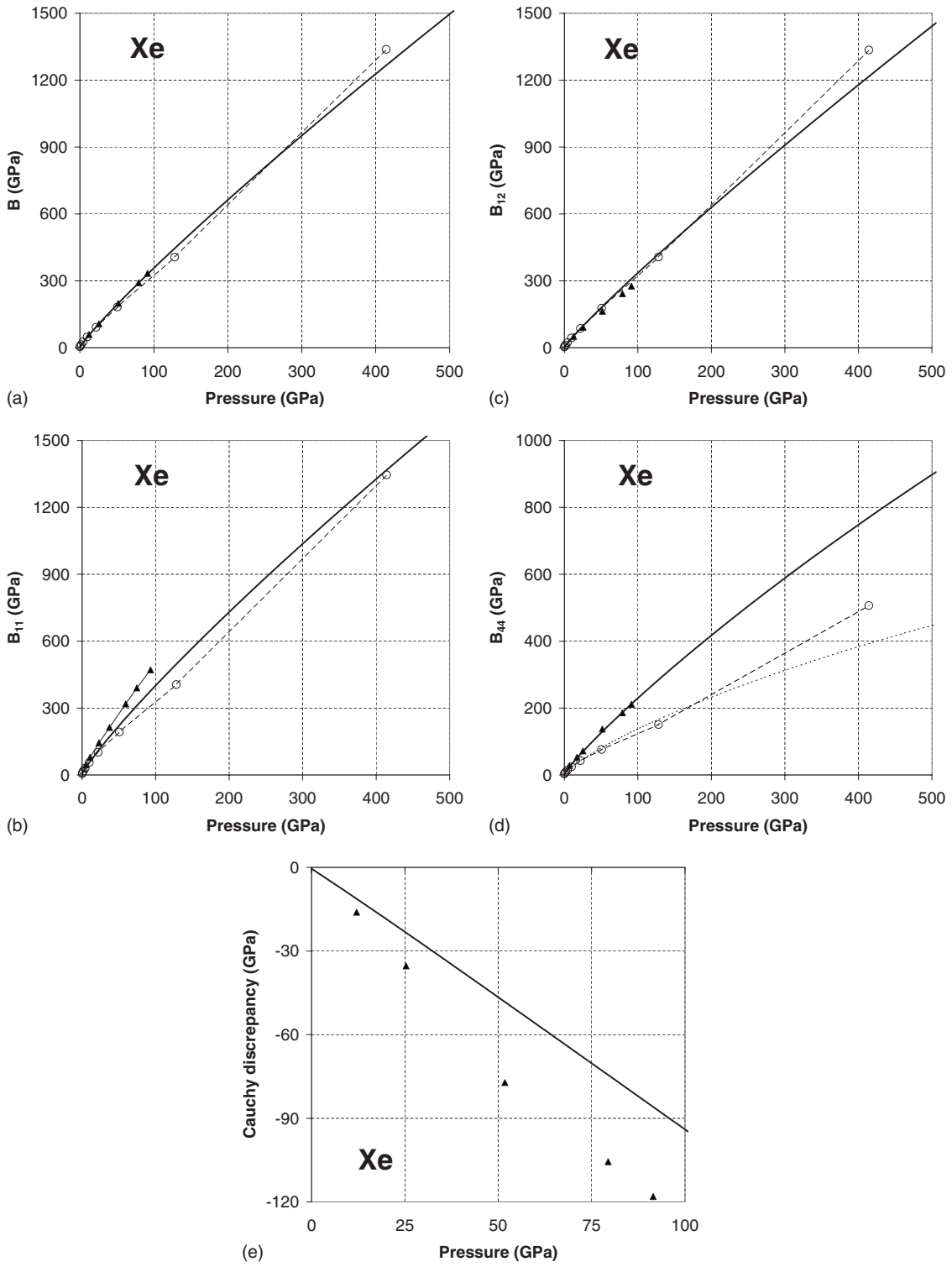

FIG. 8. Pressure-dependent effective elastic moduli [(a) B, (b) B_{11}, (c) B_{12}, (d) B_{44}] and the (e) Cauchy discrepancy of Xe, calculated with the many-body model (solid line) and the Buckingham pair potential (dotted line) at 0 K. The results are compared to 0 K *ab initio* data (Ref. 30—solid triangles) and pair-interacting model calculations (Ref. 42—dashed line).

3456, half of them initially solid and half initially liquid, in a $6\times6\times24$ fcc unit-cell configuration. The two domains, liquid and solid, are joined along the z axis.

The melting curves are calculated over a broad range of densities, differing as much as four times between the highest and the lowest densities. Density variations as large as these may cause the results to be highly dependent on the type of the cutoff function used in calculations. In order to study this dependence we constructed two different types of cutoff functions—one being constant-distance, and the other varying-distance constant-neighbor cutoff function—and compared them by calculating the melting curve of Ar. The

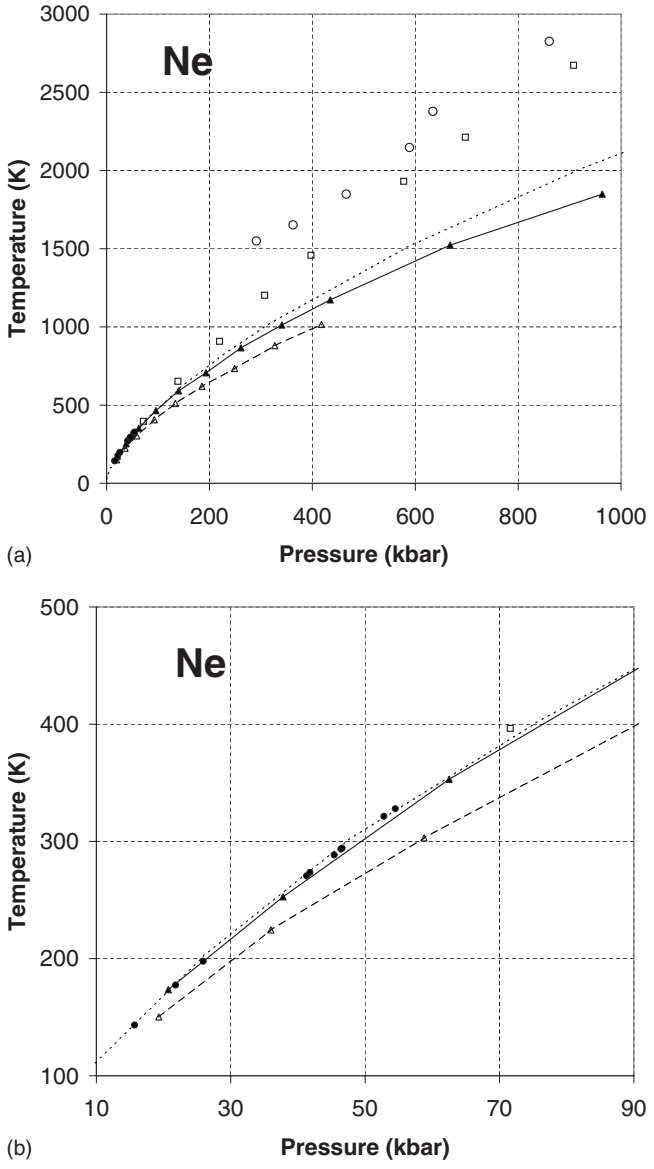

FIG. 9. The melting curve of Ne at (a) high and (b) low pressures, calculated with the many-body model (filled triangles) and the Buckingham potential (empty triangles). Filled circles represent the experimental data of Vos *et al.* (Ref. 20). Empty circles represent an *ab initio* calculation by Koči *et al.* (Ref. 38). Empty squares and the dotted line represent pair-potential calculations by the same authors (Ref. 20—Buckingham potential, Ref. 38—Lennard-Jones potential).

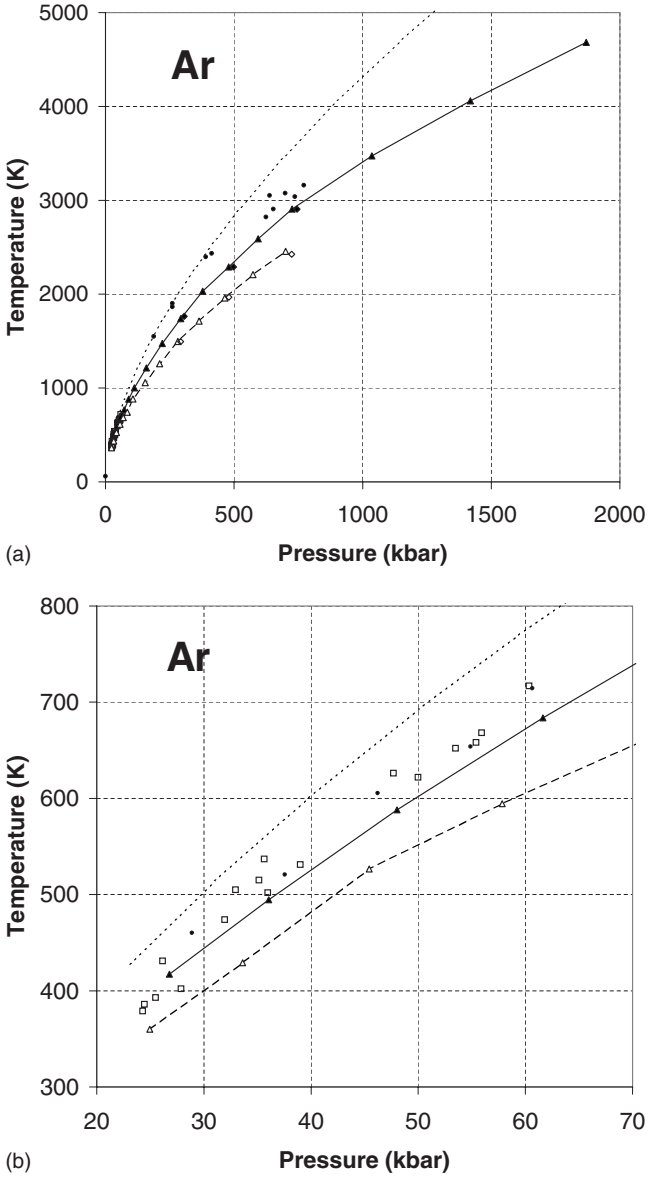

FIG. 10. The melting curve of Ar at (a) high and (b) low pressures, calculated with the many-body model (filled diamonds and triangles) and the Buckingham potential (empty diamonds and triangles). Diamonds and triangles correspond to the varying-distance and the constant-distance cutoff functions, respectively. Empty squares and dots represent the experimental data of Zha *et al.* (Ref. 21) and Boehler *et al.* (Ref. 22), respectively. The dotted line represents a pair-potential calculation by Belonoshko (Ref. 41). It can be seen that the choice of the cutoff function does not affect the results.

results appear in Fig. 10. The constant-distance cutoff function (represented with triangles) includes all atoms within the range of 1.573 zero-pressure nearest-neighbor distances and does not depend on the density. The varying-distance cutoff function (represented with diamonds), which is defined in Eq. (17), includes only atoms below the second-nearest neighbors (in the fcc lattice). As the effect of the cutoff function on the obtained results was minimal, it was decided to use the constant-distance cutoff function in all other calculations.

The melting curves of Ne, Ar, Kr, and Xe, calculated with and without the many-body term and compared to other pair potential calculations,[20,38–41] *ab initio*,[37,38] and experimental results,[20–23] are shown in Figs. 9–12. The calculated and the experimental melting curves agree at low pressures. A good illustration of this agreement can be seen in Figs. 9(b) and 10(b), where our model reproduces the low pressure (below ~70 kbar) melting curves of Ne[20] and Ar.[21,22] At higher pressures, a growing discrepancy starts to appear, with the calculated melting curves being increasingly lower than the experimental curves. In the case of Kr and Xe, the discrepancy reaches its maximum at the points of the cusps reported

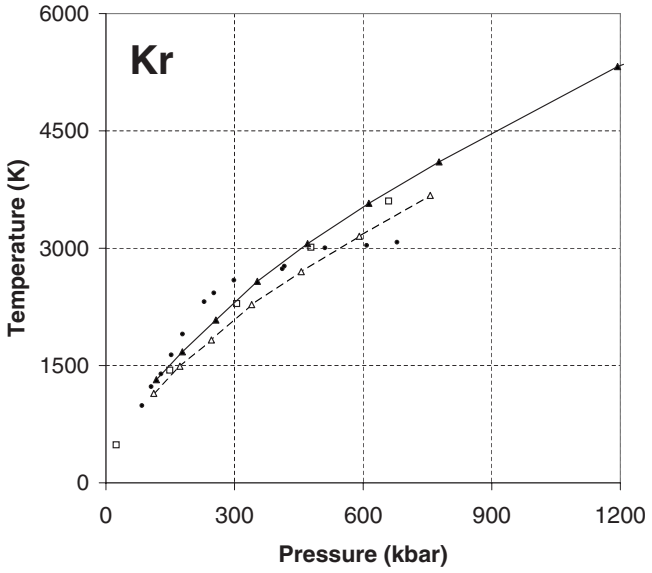

FIG. 11. The melting curve of Kr, calculated with the many-body model (filled triangles) and the Buckingham potential (empty triangles). Dots represent the experimental data of Boehler *et al.* (Ref. 22). Empty squares represent a Buckingham potential calculation by Giuffré and Saija (Ref. 40).

by Boehler *et al.*[22] The cusps themselves and the experimentally reported behavior above them are not reproduced in our calculations. It can be seen that melting curves calculated without the many-body term are systematically lower than the results of the many-body model, and the discrepancy between the two calculations increases with pressure. Evidently, the many-body term improves the agreement with experiment, bringing the calculated melting curves higher and closer to the experimental data.

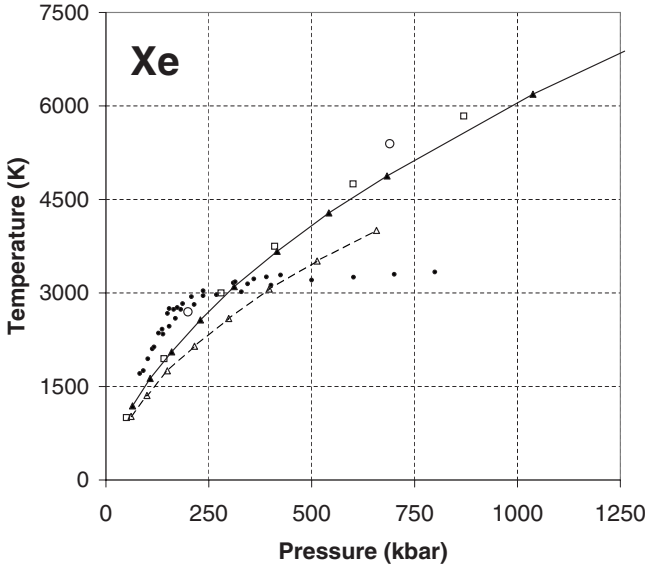

FIG. 12. The melting curve of Xe, calculated with the many-body model (filled triangles) and the Buckingham potential (empty triangles). Dots represent the experimental data of Boehler *et al.* (Refs. 22 and 23). Empty circles represent an *ab initio* calculation by Belonoshko *et al.* (Ref. 37). Empty squares represent a Buckingham potential calculation by Saija and Prestipino (Ref. 39).

Compared to other theoretical calculations, our results are consistent with most melting curves calculated with the Buckingham pair potential (Ref. 20 for Ne, Ref. 40 for Kr, and Ref. 39 for Xe), as well as with the recent *ab initio* calculation of Xe melting by Belonoshko *et al.*[37] However, our calculations are less consistent with both *ab initio* and Lennard-Jones melting curves of Ne by the same authors,[38] as well as the earlier calculations of Ar,[41] which are significantly higher than our results. One can notice the constant discrepancy between our Buckingham potential calculations and the other Buckingham calculations reported above. This is mainly caused by the difference in potential parameters, especially those affecting the bulk moduli pressure derivatives, which are lower in our calculations. Although these parameters improve the agreement with the experimental bulk moduli pressure derivatives and the zero-temperature compression curves, they decrease the melting curves, causing disagreement with experiment and previous calculations. Apparently, at high-enough pressures it is not possible to reproduce both the equation of state and the melting curve with the same set of pair-potential parameters.

V. SUMMARY AND DISCUSSION

We have developed and fitted a many-body EAM-like model to describe the atomic interactions in rare gases. The model is based on the Buckingham pair potential, fitted to experimental high-pressure compression curves of rare-gas solids, and contains a many-body term that affects the shear elastic and the thermal properties of the system. The many-body term introduces an explicit angular dependence into the model by accounting for three-body interactions. Its functional form is inspired by the MEAM formalism by Baskes,[36] though our model is less complicated and, therefore, easier to calibrate. While the many-body term of MEAM has over eight parameters, our many-body term has essentially one parameter, easily fitted to experimental and *ab initio* data. As we have shown, spherically symmetric EAM-like many-body models are insufficient to reproduce the elastic properties of rare-gas solids, such as the Cauchy discrepancy. Introducing three-body interactions, namely, an angular dependence into the model allows it to describe the Cauchy discrepancy correctly, confirming that three-body interactions are a significant element of a realistic model of rare gases. This result is consistent with previous works[10,11,29,30] that asserted the importance of three-body interactions in rare gases.

In earlier many-body models of rare gases the three-body term was used to correct the cohesion energy and the equation of state of the system. A recent example of this approach is the work of Freiman and Tretyak,[33] who used the three-body model of Loubeyre[31,32] to calculate the equations of state of rare gases at a multimegabar pressure range. We pursued an alternative approach and constructed a many-body term whose purpose was to effectively correct the elastic properties of the system without affecting the cohesion energy and the equation of state. The latter remained the same as if they were described by a pure pair potential (Buckingham, in our case). Decoupling the terms affecting

the bulk and the elastic properties of the system provided us with a clearer view of the model and its behavior, allowing better control of the model parameters.

The recent work of Aoki and Kurokawa[34] demonstrates another approach in constructing a many-body model of a rare-gas solid. The authors constructed a model many-body potential with the following general form: $\phi_{ij}(r_{ij};\bar{\rho}_i+\bar{\rho}_j)$, where $\bar{\rho}_i$ is defined according to Eq. (2). The model describes the repulsive part of the interaction and affects the elastic properties of the system. The attractive part is described with an arbitrary pair potential, such as the van der Waals potential. This is contrary to our model, where the many-body term affects *only* the elastic properties and does not affect cohesion. The model is able to reproduce the high-pressure elastic properties of Ar, including the negative Cauchy discrepancy. This is due to the explicit dependence of the many-body potential ϕ_{ij} on the interatomic distance r_{ij}. Without this dependence ϕ_{ij} becomes similar to the "embedding energy" $F(\bar{\rho}_i)$ of the spherically symmetric EAM model, which is unable to reproduce the negative Cauchy discrepancy.

Comparing our calculations to other theoretical approaches, one can see that in the case of isotropic bulk properties, namely, the zero-temperature compression curve and the pressure dependence of the bulk modulus [Figs. 1–4 and 5(a)–8(a)], most of the models produce comparable results in the experimental range and successfully reproduce the experimental data. This is not the case with the pressure dependence of the individual elastic constants, both experimental and *ab initio*, which are successfully reproduced with the many-body models, but not with the pair-interacting models. In particular, the pressure dependence of the C_{44} elastic constant, which is fitted exactly in our model, is much lower than both experimental and *ab initio* results when calculated with the Buckingham potential alone without the many-body term. An important result of the correct description of high-pressure elastic constants in our model is the ability to reproduce the negative Cauchy discrepancy of high-pressure rare-gas solids, which is seen both in experiments and *ab initio* calculations. This result can be obtained neither with pair potentials, which have zero Cauchy discrepancy, nor with spherically symmetric EAM-like many-body models. It should be noted that the Lennard-Jones potential, which suffers from incorrect bulk modulus pressure dependence, was unable to reproduce any data plausibly.

Discrepancies between the different models become more significant above the experimental range. For example, Freiman and Tretyak reported that their model equation of state exhibits unphysical inflection points at 250, 200, and 175 GPa for Ar, Kr, and Xe, respectively. Since our model equation of state is not affected by the three-body term, these phenomena are not seen in our results. Another example is the pressure dependence of the elastic constants, with our results exhibiting a negative curvature, which is nonexistent in the other models.

A significant drawback of the current model is its inability to capture the high-pressure fcc-hcp transition, seen experimentally in Xe and Kr.[15–18] In our model, the cohesion energy, described by a second-nearest-neighbor pair potential, is identical for fcc and hcp. This is contrary to Loubeyre's approach, where the three-body term affects the cohesion energy and makes the fcc-hcp transition possible. According to recent experiments[17,18] the volume difference between fcc and hcp is below 1.5%, and the difference between the bulk moduli of the two phases is also small. These experiments suggest the existence of a large mixed phase region, where both phases are mechanically stable. Recent *ab initio* calculations[30,44] also suggest that the fcc phase in Xe is mechanically stable up to 1 Mbar at the least. Based on these considerations we allowed ourselves to disregard the above-mentioned transition in the course of this work and treated both phases as fcc. However, further improvement of the model should include a mechanism for an fcc-hcp transition.

According to Boehler,[22,23] the experimental melting curves of heavy rare gases (Ar, Kr, and Xe) change their slope dramatically, leading to creation of cusps. At present, their origin remains controversial despite the various proposed explanations. The latter includes an fcc-bcc transformation prior to melting[25,39] and a $5p$-d hybridization leading to formation of clusters with icosahedral short-range order (ISRO) in the liquid.[23] Previous calculations, both model (using pair potentials) (Refs. 20, 25, and 39–41) and *ab initio*,[37,38] have not shown these cusps; our calculations have not shown them either. However, below the cusps, our model melting curves agree with the experimental data better than the melting curves calculated with the Buckingham potential, and in agreement with recent *ab initio* calculations (Ref. 37). Evidently, for a given pair potential, the many-body term improves the agreement with experiment.

To summarize, the present many-body model has succeeded in representing the elastic and the thermal properties of rare-gas solids, including the Cauchy discrepancies and the melting curves at lower pressures. However, in order to study more complex phenomena, such as the melting curve cusps or the fcc-hcp phase transition, further development of the model is needed.

APPENDIX

The procedure we use to calculate the pressure dependence of the elastic constants includes a numerical evaluation of the second derivatives of the system energy with regard to the appropriate infinitesimal strain. The strain that needs to be applied in each calculation is conveniently defined via the metric tensor G. The metric tensor of an isotropically compressed undistorted cubic crystal is

$$G_0 = V^{2/3}\begin{pmatrix} 1 & 0 & 0 \\ 0 & 1 & 0 \\ 0 & 0 & 1 \end{pmatrix}, \tag{A1}$$

where V is the equilibrium crystal volume corresponding to hydrostatic pressure P. The formulae used to calculate the elastic constants and the metric tensors corresponding to the appropriate infinitesimal strains appear below. Here $E(G)$ is the energy of a system with a given G and ε is the infinitesimal parameter, which is equal to 10^{-4} in our calculations.

C_{11} is calculated according to the following formula:

$$C_{11} = \frac{E(G_+) + E(G_-) - 2E(G_0)}{V\varepsilon^2} + P \tag{A2}$$

and

$$G_+ = V^{2/3}\begin{pmatrix} (1+\varepsilon)^2 & 0 & 0 \\ 0 & 1 & 0 \\ 0 & 0 & 1 \end{pmatrix},$$

$$G_- = V^{2/3}\begin{pmatrix} (1-\varepsilon)^2 & 0 & 0 \\ 0 & 1 & 0 \\ 0 & 0 & 1 \end{pmatrix}. \tag{A3}$$

C_{12} is calculated as follows:

$$C_{12} = \frac{E(G_{++}) + E(G_{--}) - E(G_{+-}) - E(G_{-+})}{4V\varepsilon^2}, \tag{A4}$$

with

$$G_{++} = V^{2/3}\begin{pmatrix} (1+\varepsilon)^2 & 0 & 0 \\ 0 & (1+\varepsilon)^2 & 0 \\ 0 & 0 & 1 \end{pmatrix},$$

$$G_{+-} = V^{2/3}\begin{pmatrix} (1+\varepsilon)^2 & 0 & 0 \\ 0 & (1-\varepsilon)^2 & 0 \\ 0 & 0 & 1 \end{pmatrix},$$

$$G_{--} = V^{2/3}\begin{pmatrix} (1-\varepsilon)^2 & 0 & 0 \\ 0 & (1-\varepsilon)^2 & 0 \\ 0 & 0 & 1 \end{pmatrix},$$

$$G_{-+} = V^{2/3}\begin{pmatrix} (1-\varepsilon)^2 & 0 & 0 \\ 0 & (1+\varepsilon)^2 & 0 \\ 0 & 0 & 1 \end{pmatrix}. \tag{A5}$$

Finally, C_{44} is

$$C_{44} = \frac{E(G_{\nearrow}) + E(G_{\nwarrow}) - 2E(G_0)}{V\varepsilon^2}, \tag{A6}$$

where

$$G_{\nearrow} = V^{2/3}\begin{pmatrix} 1 & 0 & 0 \\ 0 & 1 & \varepsilon \\ 0 & \varepsilon & 1 \end{pmatrix},$$

$$G_{\nwarrow} = V^{2/3}\begin{pmatrix} 1 & 0 & 0 \\ 0 & 1 & -\varepsilon \\ 0 & -\varepsilon & 1 \end{pmatrix}. \tag{A7}$$

[1] See Refs. 2, 4–33, 35–40, and 43 below.
[2] A. P. Jephcoat, Nature (London) **393**, 355 (1998).
[3] R. Boehler, Rev. Geophys. **38**, 221 (2000).
[4] K. Syassen and W. B. Holzapfel, Phys. Rev. B **18**, 5826 (1978).
[5] K. Asaumi, Phys. Rev. B **29**, 7026 (1984).
[6] A. N. Zisman, I. V. Aleksandrov, and S. M. Stishov, Phys. Rev. B **32**, 484 (1985).
[7] A. Polian, J. M. Besson, M. S. Grimsditch, and W. A. Grosshans, Phys. Rev. B **39**, 1332 (1989).
[8] A. Polian, J. P. Itie, E. Dartyge, A. Fontaine, and G. Tourillon, Phys. Rev. B **39**, 3369 (1989).
[9] L. W. Finger, R. M. Hazen, G. Zou, H. K. Mao, and P. M. Bell, Appl. Phys. Lett. **39**, 892 (1981).
[10] M. Grimsditch, P. Loubeyre, and A. Polian, Phys. Rev. B **33**, 7192 (1986).
[11] H. Shimizu, H. Tashiro, T. Kume, and S. Sasaki, Phys. Rev. Lett. **86**, 4568 (2001).
[12] R. J. Hemley, C. S. Zha, A. P. Jephcoat, H. K. Mao, L. W. Finger, and D. E. Cox, Phys. Rev. B **39**, 11820 (1989).
[13] H. Shimizu, N. Saitoh, and S. Sasaki, Phys. Rev. B **57**, 230 (1998).
[14] H. Shimizu, H. Imaeda, T. Kume, and S. Sasaki, Phys. Rev. B **71**, 014108 (2005).
[15] A. P. Jephcoat, H.-k. Mao, L. W. Finger, D. E. Cox, R. J. Hemley, and C.-s. Zha, Phys. Rev. Lett. **59**, 2670 (1987).
[16] K. A. Goettel, J. H. Eggert, I. F. Silvera, and W. C. Moss, Phys. Rev. Lett. **62**, 665 (1989).
[17] H. Cynn, C. S. Yoo, B. Baer, V. Iota-Herbei, A. K. McMahan, M. Nicol, and S. Carlson, Phys. Rev. Lett. **86**, 4552 (2001).
[18] D. Errandonea, B. Schwager, R. Boehler, and M. Ross, Phys. Rev. B **65**, 214110 (2002).
[19] F. Occelli, M. Krisch, P. Loubeyre, F. Sette, R. Le Toullec, C. Masciovecchio, and J. P. Rueff, Phys. Rev. B **63**, 224306 (2001).
[20] W. L. Vos, J. A. Schouten, D. A. Young, and M. Ross, J. Chem. Phys. **94**, 3835 (1991).
[21] C. S. Zha, R. Boehler, D. A. Young, and M. Ross, J. Chem. Phys. **85**, 1034 (1986).
[22] R. Boehler, M. Ross, P. Soderlind, and D. B. Boercker, Phys. Rev. Lett. **86**, 5731 (2001).
[23] M. Ross, R. Boehler, and P. Soderlind, Phys. Rev. Lett. **95**, 257801 (2005).
[24] L. Verlet, Phys. Rev. **159**, 98 (1967).
[25] A. B. Belonoshko, R. Ahuja, and B. Johansson, Phys. Rev. Lett. **87**, 165505 (2001).
[26] R. A. Aziz and H. H. Chen, J. Chem. Phys. **67**, 5719 (1977).
[27] M. V. Bobetic and J. A. Barker, Phys. Rev. B **2**, 4169 (1970).
[28] D. C. Wallace, *Thermodynamics of Crystals* (Wiley, New York, 1972).
[29] T. Iitaka and T. Ebisuzaki, Phys. Rev. B **65**, 012103 (2001).
[30] T. Tsuchiya and K. Kawamura, J. Chem. Phys. **117**, 5859 (2002).
[31] P. Loubeyre, Phys. Rev. Lett. **58**, 1857 (1987).
[32] P. Loubeyre, Phys. Rev. B **37**, 5432 (1988).
[33] Yu. A. Freiman and S. M. Tretyak, Low Temp. Phys. **33**, 719 (2007).

[34] M. Aoki and T. Kurokawa, J. Phys.: Condens. Matter **19**, 236228 (2007).
[35] M. S. Daw and M. I. Baskes, Phys. Rev. B **29**, 6443 (1984).
[36] M. I. Baskes, Phys. Rev. B **46**, 2727 (1992).
[37] A. B. Belonoshko, S. Davis, A. Rosengren, R. Ahuja, B. Johansson, S. I. Simak, L. Burakovsky, and D. L. Preston, Phys. Rev. B **74**, 054114 (2006).
[38] L. Koci, R. Ahuja, and A. B. Belonoshko, Phys. Rev. B **75**, 214108 (2007).
[39] F. Saija and S. Prestipino, Phys. Rev. B **72**, 024113 (2005).
[40] E. Giuffre and F. Saija, Atti Accad. Peloritana Pericolanti, Cl. Sci. Fis., Mat. Nat. **85**, C1A0701001 (2007).
[41] A. B. Belonoshko, High Press. Res. **10**, 583 (1992).
[42] E. V. Zarochentsev, V. N. Varyukhin, E. P. Troitskaya, Val. V. Chabanenko, and E. E. Horbenko, Phys. Status Solidi B **243**, 2672 (2006).
[43] J. R. Morris, C. Z. Wang, K. M. Ho, and C. T. Chan, Phys. Rev. B **49**, 3109 (1994).
[44] J. K. Dewhurst, R. A. Ahuja, S. Li, and B. Johansson, Phys. Rev. Lett. **88**, 075504 (2002).